Effect of evaporation cooling on drying capillary active building materials

Michele Bianchi Janetti [a, *], Luigi P.M. Colombo [b], Fabian Ochs [a], Wolfgang Feist [a, c]

[a] University of Innsbruck, Department of Structural Engineering and Material Sciences, Unit of Energy Efficient Building, Technikerstr. 13, 6020 Innsbruck, Austria
[b] Dipartimento di Energia, Politecnico di Milano, via Lambruschini 4, 20156 Milano, Italy
[c] Passivhaus Institut Dr. Wolfgang Feist, Rheinstr. 44/46, 64283 Darmstadt, Germany

The relevance of evaporation cooling on drying capillary active building materials is investigated through numerical simulation and non-destructive measurements. The drying rate results to be strongly related to the so-called wet bulb temperature, i.e. the temperature reached inside the sample during the early drying phase. It is shown that the faster the process occurs, the lower is the wet bulb temperature. The experiments are carried out inside a climatic chamber under controlled atmospheric conditions (temperature and relative humidity), using calcium silicate samples. The drying rates are determined by weight- ing the samples during time, while the surface temperature is measured via infrared thermography. A mathematical model describing transient heat and moisture transfer is implemented with the software COMSOL for 3D-simulation, and afterward validated by comparison with the measured data. The numeri- cal solution presents a satisfactory agreement with the experimental results. A sensitivity analysis is also performed for different input parameters including convective heat transfer coefficient and uncertainties in material properties. The validated model is then used for simulation of a set of drying cases by varying the sample thickness and boundary conditions. Hence, the water content distribution inside the samples is investigated by determining boundary conditions and sample dimensions, in which nearly uniform wa- ter content can be obtained. In fact, uniform distribution is a prerequisite for an experimental method, recently studied by the authors, that aims at determining the water retention curve of capillary active materials by means of drying tests.,

Keywords: Capillary active materials Calcium silicate, Heat and mass transfer, Infrared thermography, COMSOL

1. Introduction

In order to properly design building components, a thorough knowledge of heat and moisture transfer in the employed materials is necessary. This is particularly important if a thermal insulation is applied on the interior side of the building, since in this case the risk of moisture damages may be pronounced. The increasing interest in this field is proved by numerous recent studies concerning both modeling and experimental research (e.g. [1–9]). This work aims at extending the current knowledge by investigating the drying behavior of calcium silicate, which is widely used as insulation material due to its favorable hygrothermal properties [2,3,10,11]. To this aim, experiments and numerical simulations are carried out.

Article history:
Received 2 May 2017
Revised 15 December 2017
Accepted 20 December 2017
Available online 27 December 2017

Drying tests are often employed for determination of important material properties and are typically less time-consuming than other procedures performed to the same aim at steady state conditions (see e.g. [12]). These material properties are the liquid water diffusivity and the water retention curve, which describe the capability of a porous material to transport water via capillary action and to retain moisture inside its cavities, respectively. The water retention curve gives the local water content as a function of the local relative humidity, while the water diffusivity depends on the water content itself. Furthermore, besides their employment for material characterization, drying experiments are also a useful benchmark for hygrothermal models, as clarified later on.

The above mentioned applications have been already addressed in numerous studies [11,13–25]. In [14–16], a method for the characterization of the water diffusivity was proposed, while in [26] the water retention curve was determined by measuring both water content and relative humidity during drying at different

* Corresponding author.
E-mail address: michele.janetti@uibk.ac.at (M. Bianchi Janetti).

Published Journal Article available at: https://doi.org/10.1016/j.enbuild.2017.12.048

Nomenclature

a	parameter Eq. (B.4) (–)
c	heat capacity (J/(kg °C))
C	parameter Eq. (B.6) (W/(m K^4))
D	diffusivity (m^2/s)
h	specific enthalpy (J/kg)
H	volumetric enthalpy (J/m^3)
m	mass (kg)
m;n	parameters Eq. (B.3) (–)
$\mathbf{n}$	normal unit vector
N	number of specimens
$\mathbf{j}$	mass flux (kg/(m^2 s))
k_1;k_2	parameters Eq. (B.1) (Pa); (–)
K_{ij}	transfer parameter
p	pressure (Pa)
$\dot{\mathbf{q}}$	heat flux (W/m^2)
R	gas constant (J/(kg K))
T	absolute temperature (K)
u	water content (kg/m^3)
x;y;z	coordinates (m)
∇	nabla operator (1/m)
α	heat transfer coeff. (W/(m^2 K))
β	mass transfer coeff. (s/m)
η	viscosity (kg/(m s))
λ	thermal conductivity (W/(m K))
ζ	parameter Eq. (B.2) (–)
θ	Celsius temperature (°C)
μ	diffusion res. factor (–)
ξ	parameter Eq. (B.2) (m)
ρ	density (kg/m^3)
σ	surface tension (N/m)
φ	relative humidity (–)
ψ	porosity (–)
Ω	porous domain (m^3)
$\partial\Omega$	boundary surface (m^2)

Subscripts

a	air
c	convective
dry	dry material
eff	effective
f	free saturation
i;j	indexes
I;II	parallel, series
p	constant pressure
rad	radiative
s	saturation, surface
sm	solid matrix
v	water vapor
w	liquid water
0	initial
∞	in the surrounding air

positions inside a material sample. Other experimental procedures (e.g. [17,18,27,28]) are based on the evidence that the temperature and relative humidity at the sample surface are connected. Typically, the surface temperature decreases at the beginning of drying, approaching the so-called wet bulb temperature. Then, after a period of time during which the process is nearly isothermal, the temperature increases again until equilibrium with the air conditions is reached. A similar but inverse behavior can be observed for the relative humidity, which remains nearly constant during the early drying period, while afterward decreases, approaching the value in the surrounding air. It has been shown that, if both temperature and water content trends are known, the water retention curve can be determined. This approach may be advantageous, since the surface temperature is measurable via infrared thermography (IRT), with a low impact on the process itself.

Despite the mentioned advantage however, a challenge arises since the water content cannot be easily assessed at the sample surface. Hence, a relation connecting the mean value of water content inside the sample to its surface value is required. In [18], this challenge was addressed by employing a lumped parameter approach and thus considering uniform moisture inside the sample during drying. In general, this condition is verified just during the early drying period, while deviations may occur later on between internal and surface values. Moreover, the moisture distribution is influenced by the sample dimensions and boundary conditions (temperature and relative humidity of the drying air, heat and mass transfer coefficients), which have to be properly designed. With respect to this issue, the use of numerical simulation may be profitable. Thus, a model able to reproduce moisture and temperature distributions is required.

Although numerous studies were recently published on hygrothermal modeling (e.g. [11,19–25]), the drying process still represents a challenge for numerical simulation. On the one hand, the material functions (water retention curve and diffusivity) may be highly non-linear at saturation. Complex mass transport mechanisms, namely capillary transport and vapor diffusion, are involved. On the other hand, 3D-geometry and realistic boundary conditions have to be considered in order to adequately reproduce the drying behavior [20,25]. It has also to be noted that uncertainties on the input parameters (i.e. material properties and boundary conditions) are in general important and a validation of the model against experimental outcomes is necessary [23,24].

According to the above statements, this study has a double purpose. First, a model for coupled heat and moisture transfer is implemented and validated against measured data. For validation of the model, experiments at different ambient conditions are carried out. Drying rates are determined by weighting the sample during time, while the surface temperature is measured via infrared thermography. The material functions used as input for the transient simulation are taken from previous studies [29,30], in which the water retention curve and the vapor diffusion resistance factor were measured by means of desiccators and vapor diffusion tests, respectively, while the water diffusivity was determined employing a peculiar method based on heat flux measurements. Hence, the results reported here represent also an additional verification for those works.

The second purpose of the paper is to determine boundary conditions and sample dimensions, in which nearly uniform water content can be obtained. To this aim, the validated model is employed for simulation of a set of drying cases, by varying the sample thickness and boundary conditions.

2. Experimental setup and boundary conditions

Initially saturated calcium silicate samples are dried until equilibrium with the surrounding air conditions is reached. The tests are carried out inside a climatic chamber where the air temperature and relative humidity are controlled by means of a ventilation system. The experimental setup and the sample schematic are shown in Fig. 1. The water content inside a sample is determined by recording its mass loss during time. To this aim, a balance with a repeatability of ±0.001 g is used. Hence, the mean value of the drying rate $\dot{m}_w = dm_w/\mathrm{d}t$ for a set of N samples is calculated as follows:

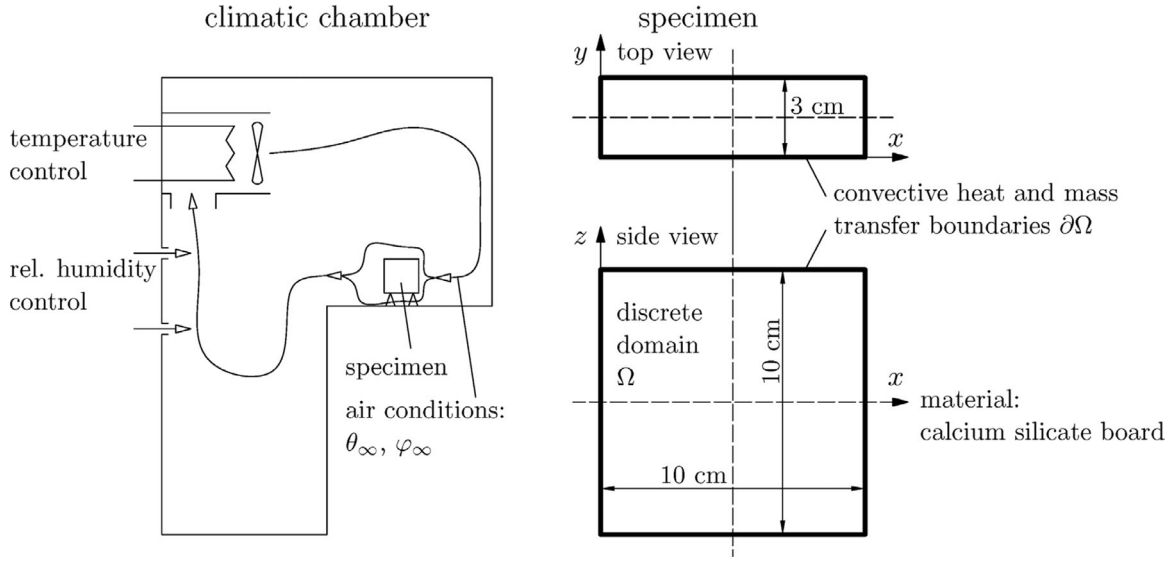

Fig. 1. Climatic chamber and specimen schematic.

$$\dot{m}_w\left(t^i+\frac{t^{i+1}-t^i}{2}\right)=\frac{\sum_{j=1}^{N}\left|\left(m_{w,j}^{i+1}-m_{w,j}^{i}\right)/\left(t^{i+1}-t^i\right)\right|}{N} \tag{1}$$

where t^i represents the time of the ith measurement and m_w the mass of water inside the sample.

In order to determine the surface temperature of the sample, an infrared camera calibrated with respect to known temperatures is employed. The experiment is repeated with different boundary conditions reported in Table 1.

Note that the heat and mass transfer coefficients, which are required as model inputs, are assumed to be constant during time and uniform at the sample surface. This assumption, which may be not always accurate according to other authors [19–21], is indeed acceptable for the considered cases, as discussed later on in Section 4. Moreover, the heat and mass transfer coefficients are connected through the Lewis analogy and can be calculated as follows:

$$\alpha=\alpha_c+\alpha_{\text{rad}} \tag{2}$$

$$\beta=\frac{1}{R_v T}\frac{\alpha_c}{\rho_a c_{p,a}}\text{Le}^{-\frac{2}{3}} \tag{3}$$

where α_c and α_{rad} are the convective and radiative heat transfer coefficients, respectively, R_v is the individual gas constant of water, T the absolute temperature, ρ_a the air density, $c_{p,a}$ the air heat capacity and Le the Lewis number. The value $\alpha_{\text{rad}}\approx 5\,\text{W/(m}^2\,\text{K)}$, approximately determined by means of correlations reported e.g. in [13,31], can be considered sufficiently accurate for the temperature range considered here. Hence, the average values of the heat and mass transfer coefficients (α_c, β) reported in Table 1 are obtained through inverse procedure, by searching for the best fit between the measured drying rates and the results of the numerical model described afterward in Section 3. The different values of the convective coefficients characterizing the three cases may be explained considering deviations in the fan operation and a slightly different positioning of the samples inside the chamber.

Table 1
Boundary and initial conditions for the considered cases. Number of samples N employed for each experiment. Mass transfer coefficient β calculated with Eq. (3) at $\theta=25\,°\text{C}$.

Case	θ_∞ (°C)	φ_∞ (–)	α_c (W/(m² K))	α_{rad} (W/(m² K))	β (s/m)	θ_0 (°C)	φ_0 (–)	N (–)
bc 1	23.5	0.52	4.32	5	2.86×10^{-8}	23.5	1	3
bc 2	25.0	0.40	6.84	5	4.51×10^{-8}	23.5	1	2
bc 3	30.0	0.35	12.60	5	8.31×10^{-8}	23.5	1	6

3. Mathematical model

In this section the mathematical model employed for coupled heat and moisture transfer is described. Hence, the numerical setup used for simulation is discussed.

3.1. Driving equations

In order to describe the coupled transfer of energy and moisture inside the sample, a well established continuum approach is employed, according to numerous authors (e.g. [32,4]). The following assumptions are made: (1) the solid phase is a rigid matrix in an inertial frame; (2) the three phase system (air, liquid water, solid) is in local equilibrium; (3) the porous medium is continuous at the macroscopic scale. Hence, by referring to a representative element of volume (REV), mean local material properties, moisture and energy states can be defined. By neglecting the flux of dry air and in absence of thermal and mass sources, the time dependent energy and moisture transfer is described by the following system:

$$\begin{cases}\dfrac{\partial H}{\partial t} &= -\nabla\cdot\left(\dot{\mathbf{q}}+h_v\mathbf{j}_v+h_w\mathbf{j}_w\right)\\ \dfrac{\partial u}{\partial t} &= -\nabla\cdot\left(\mathbf{j}_w+\mathbf{j}_v\right)\end{cases} \tag{4}$$

where H is the volumetric enthalpy specified in Appendix A, u is the local water content, and h_v and h_w are the specific enthalpies of vapor and liquid water. The total heat flux $\dot{\mathbf{q}}$, the liquid water flux $\mathbf{j}_w$ and the vapor flux $\mathbf{j}_v$ can be specified as follows, under standard temperature and pressure conditions ($p\approx1\,\text{bar}$; $0<\theta<40\,°\text{C}$), and according to several authors (e.g. [4,13]):

$$\dot{\mathbf{q}}=-\lambda_{\text{eff}}\nabla T \tag{5}$$

$$\mathbf{j}_w=-D_w\nabla u \tag{6}$$

$$\mathbf{j}_v=-\frac{1}{\mu}\frac{D_v}{R_v T}\left(p_s\nabla\varphi+\varphi\frac{\mathrm{d}p_s}{\mathrm{d}T}\nabla T\right) \tag{7}$$

where λ_{eff} is the effective thermal conductivity, including heat conduction and radiation, D_w the water diffusivity due to capillary action and μ the vapor diffusion resistance factor. Moreover, φ is the relative humidity, D_v the water vapor diffusivity in the air and p_s the saturation pressure expressed as follows [33]:

$$p_s = 610.94\, e^{\frac{17.625\theta}{243.04+\theta}} \tag{8}$$

Taking into account equations (5)–(7), system (4) can be rewritten as follows, with relative humidity and temperature as dependent variables:

$$\begin{cases} \dfrac{\partial H}{\partial T}\dfrac{\partial T}{\partial t} + \dfrac{\partial H}{\partial \varphi}\dfrac{\partial \varphi}{\partial t} = -\nabla\cdot(K_{11}\nabla T + K_{12}\nabla\varphi) \quad \text{in} \quad \Omega \\ \dfrac{\partial u}{\partial T}\dfrac{\partial T}{\partial t} + \dfrac{\partial u}{\partial \varphi}\dfrac{\partial \varphi}{\partial t} = -\nabla\cdot(K_{21}\nabla T + K_{22}\nabla\varphi) \end{cases} \tag{9}$$

with boundary and initial conditions given by the following equations:

$$\begin{aligned}(K_{11}\nabla T(\mathbf{x},t) + K_{12}\nabla\varphi(\mathbf{x},t))\cdot\mathbf{n} &= \alpha(T_\infty - T(\mathbf{x},t)) \\ &+ h_v\beta(p_{s,\infty}\varphi_\infty - p_s(T(\mathbf{x},t))\varphi(\mathbf{x},t)), \quad \mathbf{x}\in\partial\Omega\end{aligned} \tag{10}$$

$$\begin{aligned}(K_{21}\nabla T(\mathbf{x},t) + K_{22}\nabla\varphi(\mathbf{x},t))\cdot\mathbf{n} \\ = \beta(p_{s,\infty}\varphi_\infty - p_s(T(\mathbf{x},t))\varphi(\mathbf{x},t)), \mathbf{x}\in\partial\Omega\end{aligned} \tag{11}$$

$$\varphi(\mathbf{x},0) = \varphi_0, \quad \mathbf{x}\in\Omega \tag{12}$$

$$T(\mathbf{x},0) = T_0, \quad \mathbf{x}\in\Omega \tag{13}$$

where $\mathbf{n}$ is the normal unit vector pointing outward and the transport coefficients K_{ij} are:

$$K_{11} = -\lambda_{\text{eff}} - \frac{h_v\varphi D_v}{\mu R_v T}\frac{\mathrm{d}p_s}{\mathrm{d}T}; \quad K_{12} = -\frac{h_v D_v p_s}{\mu R_v T} - h_w D_w\frac{\partial u}{\partial\varphi} \tag{14}$$

$$K_{21} = -\frac{\varphi D_v}{\mu R_v T}\frac{\mathrm{d}p_s}{\mathrm{d}T}; \quad K_{22} = -\frac{D_v p_s}{\mu R_v T} - D_w\frac{\partial u}{\partial\varphi} \tag{15}$$

The material properties of calcium silicate with their assumed uncertainties are shown in Fig. 2 as functions of the relative humidity or water content. These curves have been calculated with material specific parameters, determined in previous studies and reported in Appendix B.

3.2. Implementation in a simulation software

Eqs. (9)–(13) are implemented in COMSOL (finite element method, Galerkin) by means of the PDE interface (coefficient form PDE). The choice of this software is motivated by the fact that other ones, specific for hygrothermal application [34,35], are until now limited to one or two dimensional problems. Even if COMSOL has already been employed by numerous authors for modeling coupled heat and moisture transfer (see e.g. [36–40]), a comparison with measured data for 3D drying of initially saturated samples was, to the knowledge of the authors, still lacking in the literature.

Since the heat and mass transfer coefficients are supposed uniform at all surfaces, three symmetry planes can be defined. The mapped mesh of 4000 Lagrange linear elements used for simulation is shown in Fig. 3. For discretization in time, Backward Differentiation Formula (BDF) with variable time steps is employed.

Other numerical parameters characterizing the model are reported in [41], where the quality of the numerical solution was discussed by varying the absolute and relative tolerances and the mesh refinement. It turned out that the chosen numerical setup is sufficiently accurate for the purpose of this work. Some improvement may be obtained by reducing the absolute and relative tolerances or assigning a maximum time step, whereas further mesh refinement does not lead to any significant variation of the results.

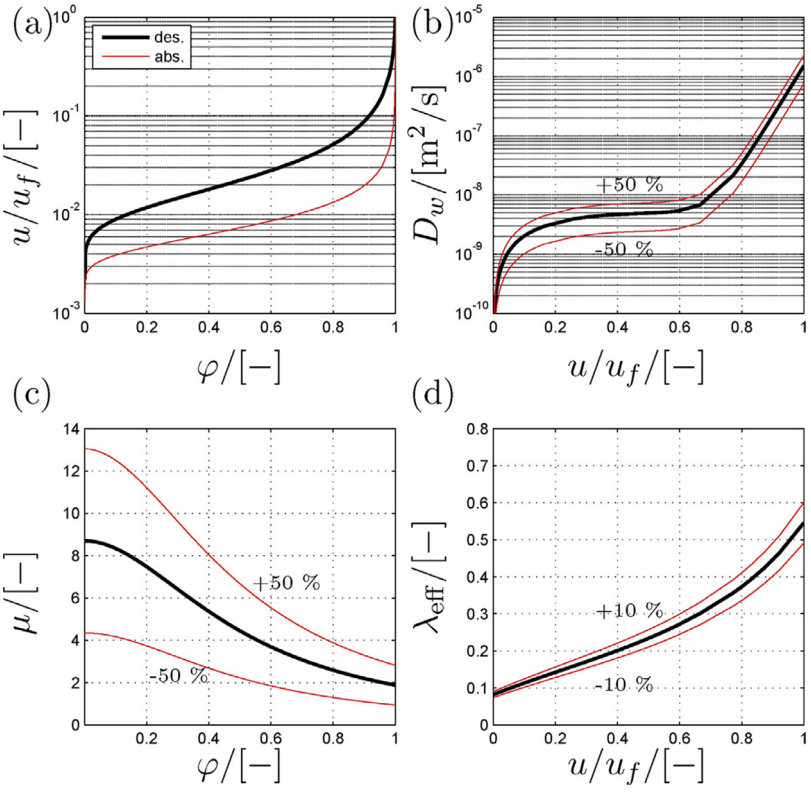

Fig. 2. (a) Water retention curve (Eq. (B.1)); (b) liquid water diffusivity (Eq. (B.2); $\theta = 20\,°\mathrm{C}$); (c) vapor diffusion resistance factor Eq. (B.3); and (d) effective thermal conductivity (Eq. (B.4); $\theta = 20\,°\mathrm{C}$. The assumed uncertainties on material functions are also shown.

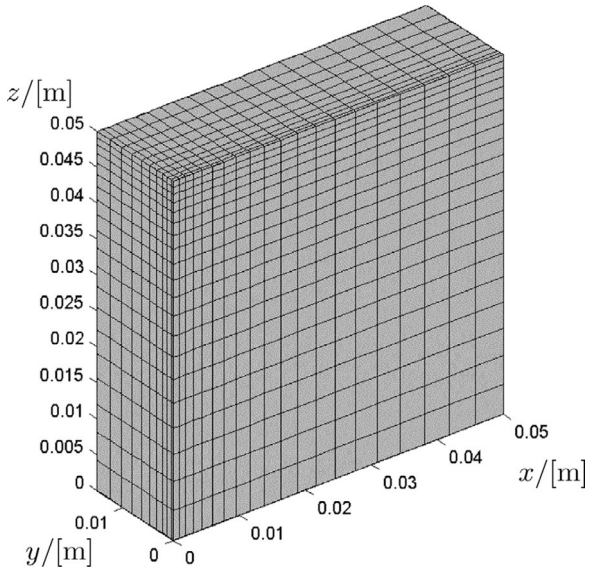

Fig. 3. 3D mesh.

Note also that the governing equations given by system (9) may lead to numerical errors in mass and energy conservation after discretization in time. This is due to the fact that the coefficients of time derivatives ($\partial u/\partial\varphi$; $\partial u/\partial T$; $\partial H/\partial\varphi$ and $\partial H/\partial T$) are functions of the dependent variables (T and φ). Even if this issue should concern both energy and mass, it may be relevant just for mass conservation, since the water retention curve $u(\varphi)$ is highly nonlinear at saturation. One way to handle this challenge is to employ the numerical scheme proposed in [41–43] (so-called mixed form). However, considering that this study focuses primarily on the description of physical processes and comparison with measurements, a detailed analysis of such numerical issues, already addressed in other works [43,44], is not included here.

4. Results

In this section, the numerical model is validated by confrontation with experimental outcomes. Hence, a sensitivity study with respect to different input parameters is performed. In the last part of the paper, the deviation between water content at the surface and inside the specimen is investigated by varying the boundary conditions and the sample thickness.

4.1. Comparison with experimental data

In Fig. 4 the measured water contents and drying rates are compared with the simulation results for the boundary conditions defined in Table 1. It can be observed that the simulation reproduces the drying behavior adequately, and a satisfactory agreement with the measured data is found.

The surface temperature has been measured for the variant "bc 2" only. The deviation between the mean value at the surface and in the surrounding air is reported in Fig. 5 (a), in which the good agreement found above between measurements and simulation results is confirmed. Fig. 5(b) shows the behavior of the mean surface relative humidity which reproduces, with opposite algebraic sign, the temperature behavior. Three phases can be observed during the whole drying process:

1. During the first phase the temperature inside the sample drops down due to evaporation, approaching the so-called wet bulb temperature. This phase is very short (≈2 h) if compared to the whole drying time, and depends on the heat capacity of the sample. Note that this early behavior is captured by the simulation but not by the measurement, due to the coarse data aquisition.
2. During the second phase, the moisture transport inside the sample occurs mainly due to capillary forces. The drying rate, temperature and relative humidity remain nearly constant.
3. The third phase presents a progressive reduction of the capillary water transport and hence of the drying rate. Vapor diffusion becomes the main mass transfer mechanism. The relative humidity and temperature at the surface evolve, by approximating the surrounding air conditions.

The three-dimensional nature of the process and the effect of cooling due to evaporation can be observed in Fig. 6 , in which the surface temperature distributions are reported at different times. The infrared plots demonstrate that, although the assumption of symmetric boundary conditions is not exactly verified, the process behavior is reproduced with sufficient agreement.

4.2. Sensitivity analysis

In this section, the sensitivity of the model with respect to the most important input parameters i.e. convective heat transfer coefficient and material properties is investigated.

In Fig. 7 the influence of the convective transfer coefficient α_c on the water content behavior and drying rates is shown. It is worth to remember here that the convective heat transfer

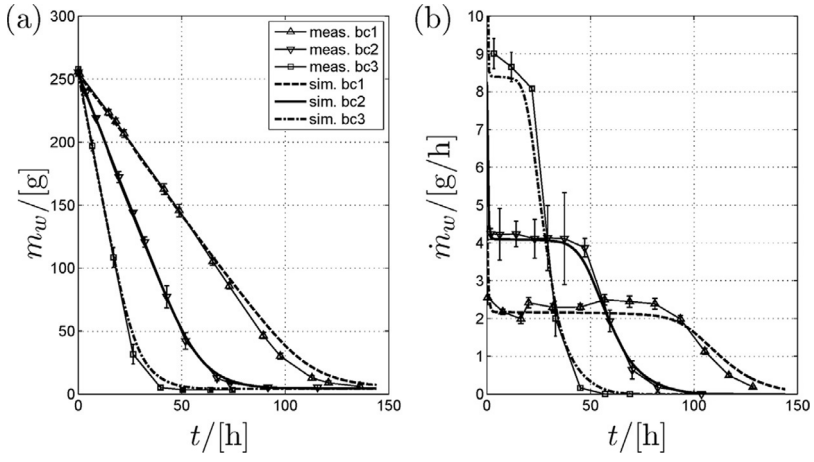

Fig. 4. (a) Water content. (b) Drying rate.

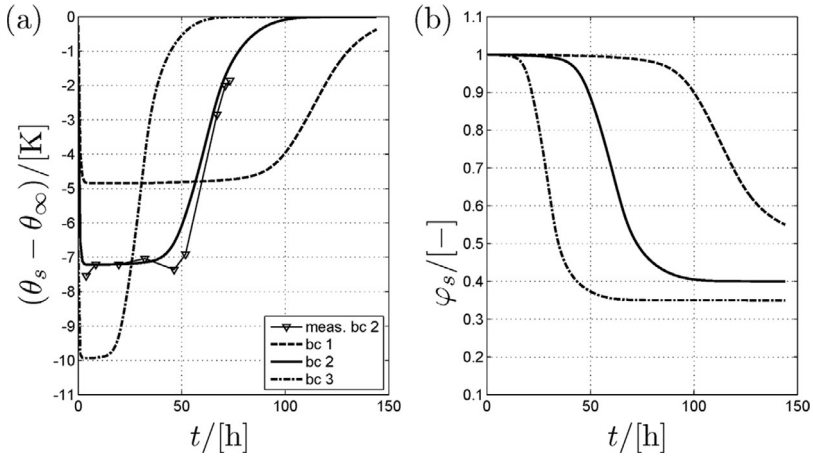

Fig. 5. (a) Deviation between mean surface temperature θ_s (at $y=0$) and air temperature θ_∞; (b) surface relative humidity (at $y=0$).

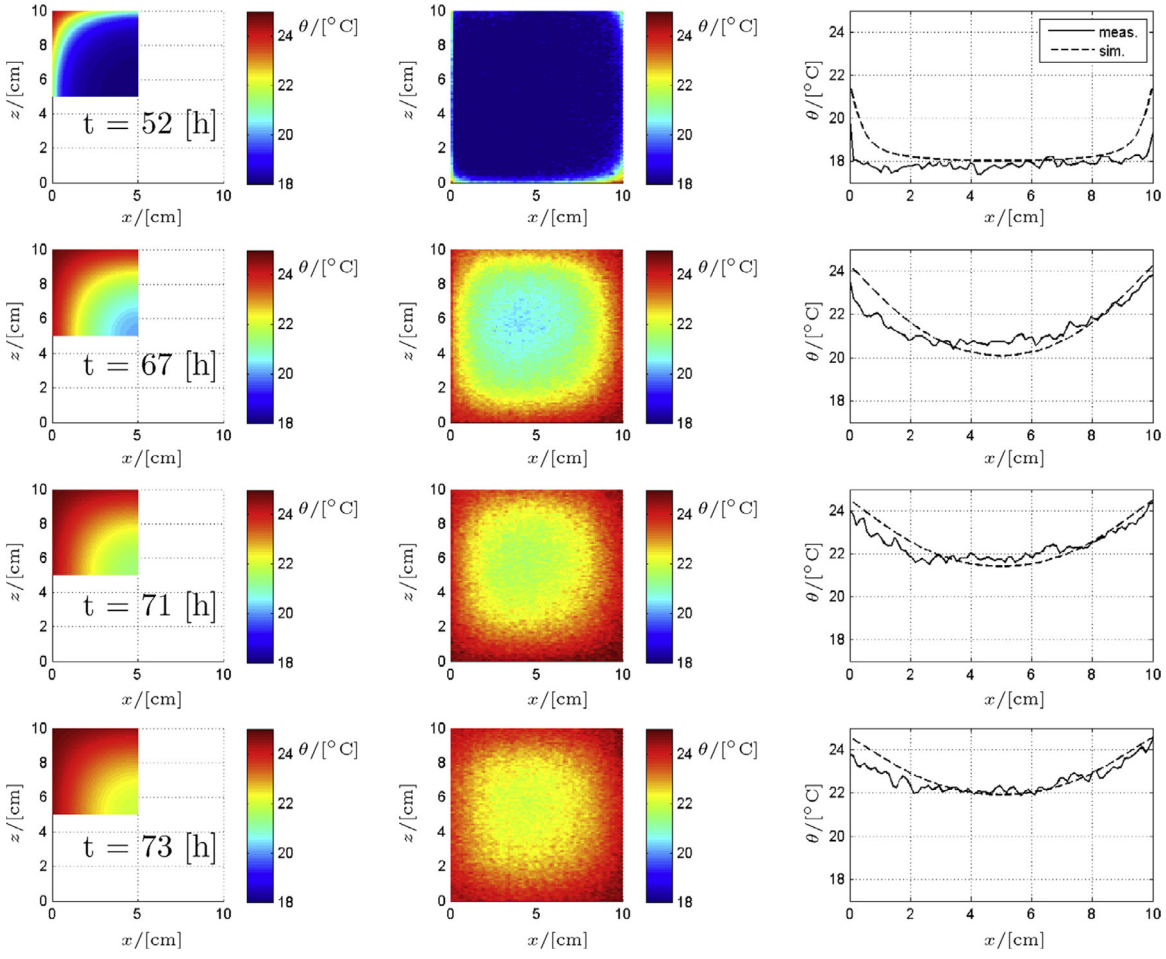

Fig. 6. Surface temperature (on the plane $y=0$) at four different times. Left: simulation results; center: measurements (infrared thermography); right: comparison between measurements and simulation at $z=5$ cm.

coefficient α_c and the mass transfer coefficient β are related through Eq. (3). In accordance with results by other authors (e.g. [9]), these parameters determine the slope of the water content trends (hence the magnitude of the drying rate) during the second, nearly isothermal, phase of drying. Considering that the convective heat transfer coefficient α_c is the only input used for the model calibration, the described experiment can also be viewed as a method for inverse determination of this parameter.

The material property presenting the most important influence in the drying process is the liquid water diffusivity. As shown in Fig. 8, its effect is negligible at the process beginning, but increases during the latter period in which it determines the steepness of the drying rate. These results are in agreement with those found in [24] for a different capillary active material (i.e. ceramic brick).

Further analysis is made by varying the water retention curve, considering two limit cases reported in Fig. 2(a). A minor in-

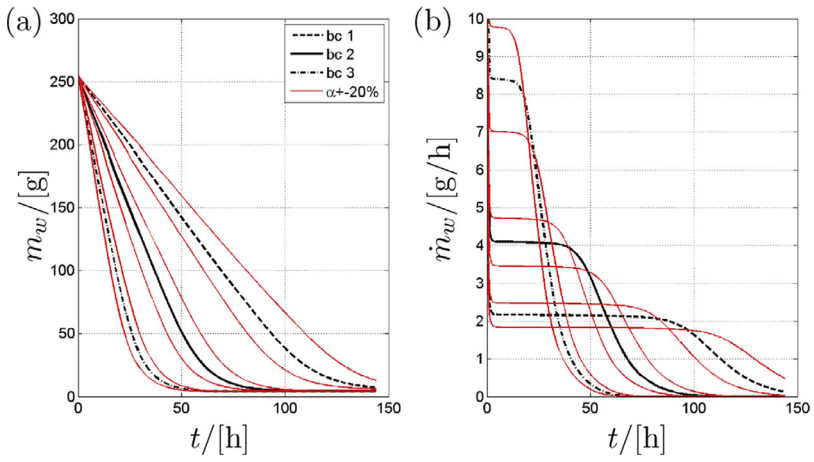

Fig. 7. Influence of the convective transfer coefficient α_c on the drying behavior (assumed uncertainty: ±20%). (a) Water content trend; (b) drying rate.

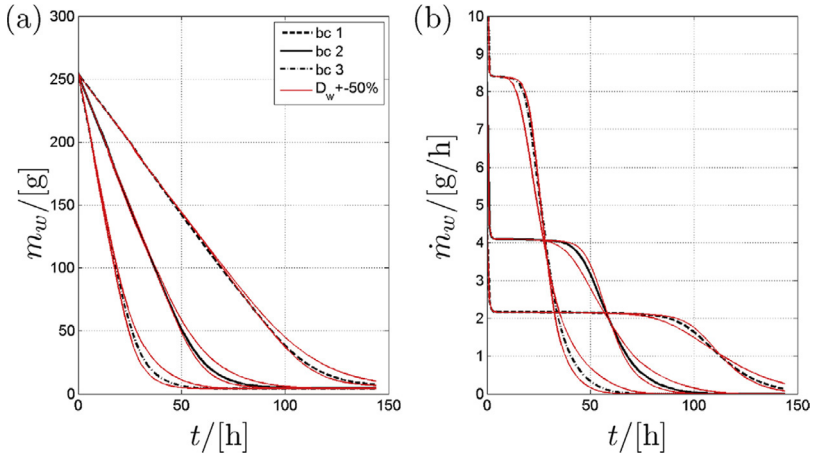

Fig. 8. Influence of the liquid water diffusivity D_w on the drying behavior (assumed uncertainty: ±50%). (a) Water content trend; (b) drying rate.

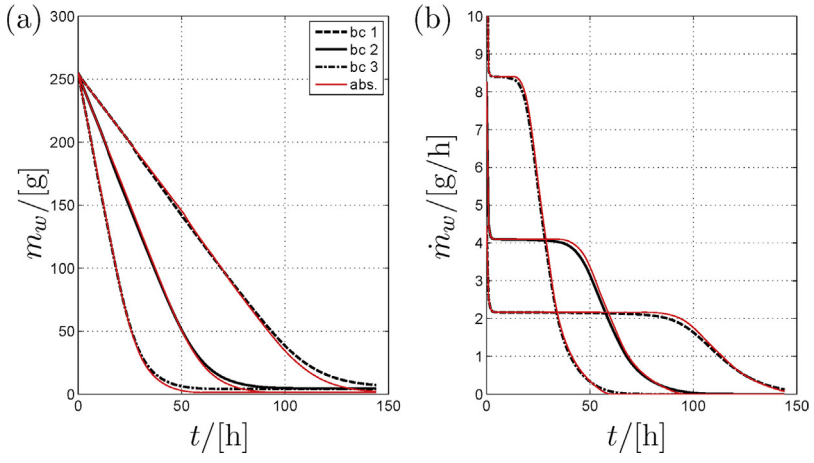

Fig. 9. Influence of the water retention curve on the drying behavior assuming two limit cases reported in Fig. 2(a). (a) Water content trend; (b) drying rate.

fluence on the simulation results has been found, as shown in Fig. 9. The low deviation between the trends is motivated by the fact that both the input functions present equal water content at saturation. A more pronounced impact has been found in [24], where however the saturation water content has also been varied. Finally, the uncertainties in vapor diffusion resistance and thermal conductivity (Fig. 2(c) and (d)) have a negligible effect on the resulting drying behaviors, which are thus not shown here.

4.3. Investigation of the water content uniformity

As stated above, the method recently proposed in [18] allows to determine the water retention curve from drying tests by means of lumped parameter analysis. This method is less time consuming than other ones used to the same aim (e.g. [12]) and involves a simple measuring equipment. The lumped parameter approach, however, requires nearly uniform water content inside the drying sample.

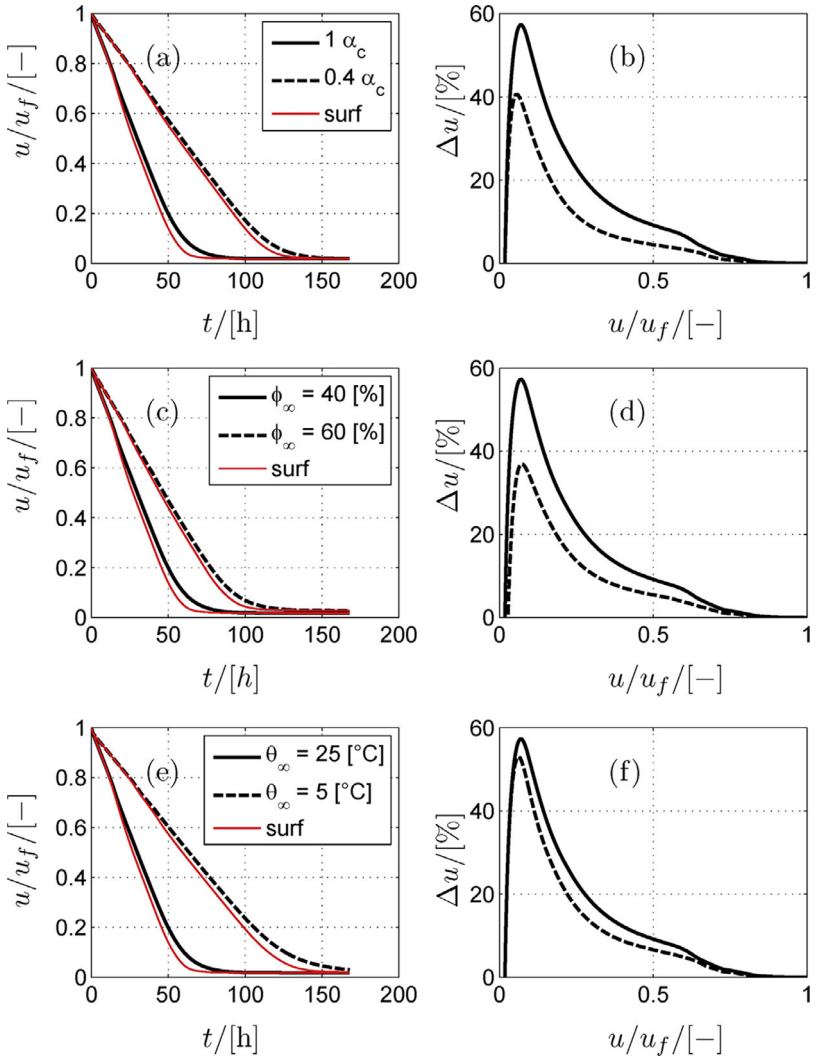

Fig. 10. Influence of the heat transfer coefficient α_c, air relative humidity φ_∞ and temperature θ_∞ on the drying trend. (a), (c), (e) Mean water content at the surface and inside the sample; (b), (d), (f), deviation between the mean water content at the sample surface and inside the sample.

In this section, the numerical model validated above is applied to determine a set of boundary conditions and sample dimensions which guarantee uniformity. To this aim, the deviation between mean water content at the surface and inside the sample is chosen as a characteristic parameter. The mean value inside the sample is calculated as the volume integral of water content divided by the sample volume. As reference case, the variant "bc 2" in Table 1 is considered, and the impact of three different input parameters is investigated. The considered parameters are: the convective heat transfer coefficient α_c, the air relative humidity φ_∞ and the air temperature θ_∞.

In Fig. 10 the simulation results are reported. The mean water content at the surface and inside the sample are shown on the left side, while on the right side the relative deviation between these two values is indicated. As expected, a reduction of α_c increases the drying time and simultaneously leads to more uniform water content (Fig. 10(a) and (b)). A similar effect is observer by increasing the relative humidity of the drying air (Fig. 10(c) and (d)). Instead, the air temperature influences the drying time significantly, but it has just a minor effect on the water content uniformity (Fig. 10(e) and f)). Note that in all considered cases the maximum relative deviation is reached at rather low water content ($u/u_f \approx 0.1$) while at high water content ($u/u_f > 0.5$) the relative deviation remains always under 10%.

According to the above results, a nearly uniform distribution inside the sample can be obtained by reducing the velocity of the drying air (hence the convective transfer coefficients for heat and mass) and by increasing its relative humidity. Both these measures, however, slow down the process drastically. Hence, in order to reduce the drying time, it may be opportune to perform the experiment at rather high temperature, since this does not significantly impact on uniformity.

Further numerical tests have been performed by varying the sample thickness. The results are shown in Fig. 11, by reporting the maximum values of the water content deviation obtained for each simulation. As expected, a reduction of the thickness determines always a more uniform water content inside the sample. It appears that, by using one centimeter thick samples with adequate boundary conditions, a maximal relative deviation lower than 20% is obtained. This represents an important improvement with respect to the preliminary study reported in [18], where a maximum relative deviation of approximately 60% was reached.

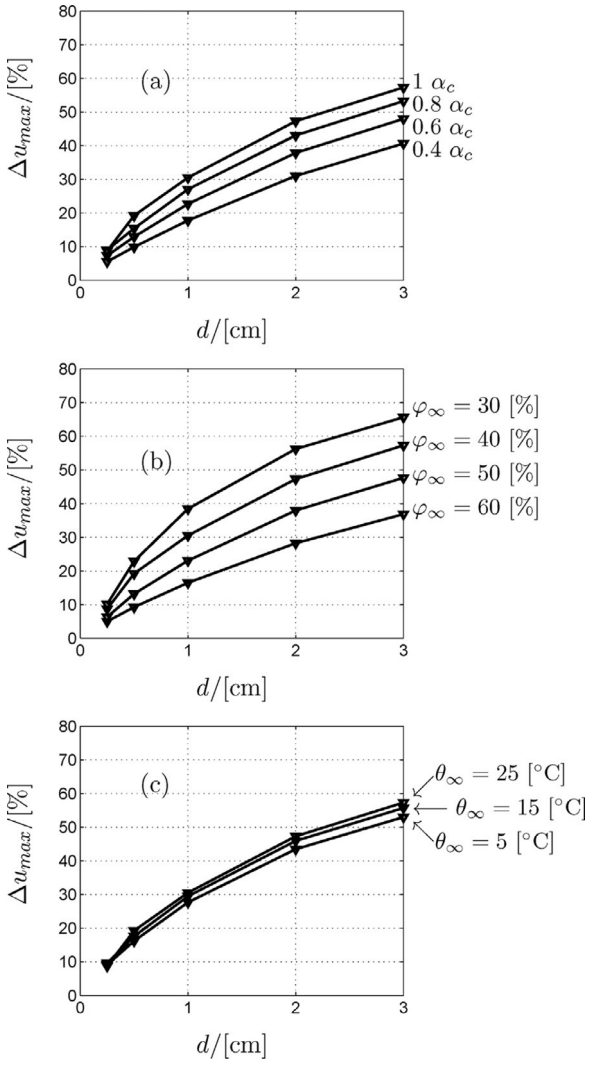

Fig. 11. Maximum deviation between the mean water content inside the sample and at the sample surface for different values of the sample thickness d. The influence of the following parameters has been investigated: (a) Convective heat transfer coefficient; (b) relative humidity of the drying air; and (c) temperature of the drying air.

5. Conclusions and outlook

This study represents a contribution for physical interpretation, mathematical modeling and experimental assessment of the drying process in capillary active materials. The main results are summarized as follows:

1. The material functions determined in [29,30] are able to reproduce the drying behavior accurately.
2. The numerical setup is adequate for simulation of initially saturated samples. The choice of temperature and relative humidity as dependent variables is adequate.
3. The sensitivity of the model with respect to uncertainties in material properties and convective transfer coefficients has been tested. The parameter presenting the major impact on the drying behavior is the convective heat transfer coefficient, whereas the most important material property is the water diffusivity.
4. The assumption of constant and uniform convective heat transfer coefficients results to be adequate, since a good agreement with the measured data is reached. The only input used for the model calibration is the convective heat transfer coefficient, which has been inversely determined.
5. The influence of boundary conditions and specimen thickness on the uniformity of water content is investigated. To this aim, the deviation between water content at the surface and inside the sample has been considered. It turned out that the convective transfer coefficient and the relative humidity of air have a large impact on both drying time and water content uniformity. On the other hand, the air temperature influences the drying time significantly, but it has just a minor impact on the uniformity of water content.
6. The method proposed in [18] for determination of the water retention curve by means of drying tests may be significantly improved by choosing optimal boundary conditions and sample dimensions.

Finally, it has to be noted that, for a more general model validation, further experiments should be performed (e.g. water-uptake experiments) since this study is limited to drying tests only.

Acknowledgments

The authors kindly thank Renato Passaniti, Dominik Granig, Andreas Saxer, Markus O. Feichter and Alireza Shantia for their support.

Appendix A.

The volumetric enthalpy of the moist material is given by the following equation:

$$H = h_{\mathrm{dry}}\rho_{\mathrm{dry}} + \psi_w(h_w\rho_w - h_{\mathrm{a}}\rho_a) + (\psi - \psi_w)h_v\rho_v \tag{A.1}$$

where ψ and ψ_w are the total porosity and the volumetric liquid water content respectively, defined as the water content divided by density of liquid water:

$$\psi = \frac{u_f}{\rho_w}; \quad \psi_w = \frac{u}{\rho_w} \tag{A.2}$$

in Eq. (A.1), h_{dry}, h_{a}, h_w and h_v represent the enthalpies of the dry material, dry air, liquid water and vapor, which are defined as follows:

$$h_{\mathrm{dry}} = c_{p,\mathrm{dry}}\theta; \quad h_{\mathrm{a}} = c_{p,\mathrm{a}}\theta \tag{A.3}$$

$$h_w = c_{p,w}\theta; \quad h_v = c_{p,v}\theta + h_{\mathrm{lv}} \tag{A.4}$$

while ρ_{dry}, ρ_a, ρ_w, ρ_v, $c_{p,\mathrm{dry}}$, $c_{p,\mathrm{a}}$, $c_{p,w}$ and $c_{p,v}$ are the densities and specific heat capacities of the dry material, dry air, liquid water and vapor and h_{lv} the specific enthalpy of vaporization.

Appendix B.

The material behavior is described by empirical functions of relative humidity and temperature. These functions are: the moisture retention curve Eq. (B.1) [45], the water diffusivity Eq. (B.2) [30], the vapor diffusion resistance factor Eq. (B.3) [46] and the effective thermal conductivity Eq. (B.4) [13]:

$$u = \frac{u_f}{1 + \left(-\rho_w R_v T \ln(\varphi)/k_1\right)^{k_2}} \tag{B.1}$$

$$D_w = \frac{\sigma_w}{\eta_w}\frac{u}{u_f}\sum_{i=1}^{2}\xi_i 10^{\zeta_i\left(\frac{u}{u_f}-1\right)} \tag{B.2}$$

$$\mu = \frac{\mu_{\mathrm{dry}}}{m\varphi^n + 1} \tag{B.3}$$

Table B.1
Material properties and model parameters.

Ref.	Description	Par.	Unit	Value
[34]	Vapor gas constant	R_v	J/(kg K)	462
[34]	Vapor diffusivity in air	D_v	m^2/s	2.66×10^{-5}
	Vapor heat capacity	$c_{p,v}$	J/(kg °C)	1864
[34]	Specific enthalpy of vaporization	h_{lv}	J/kg	2.45×10^6
	Air density	ρ_a	kg/m^3	1.2
	Air heat capacity	$c_{p,a}$	J/(kg °C)	1005
	Air thermal conductivity	λ_a	W/(m K)	0.025
	Liquid water density	ρ_w	kg/m^3	1000
	Liquid water heat capacity	$c_{p,w}$	J/(kg °C)	4186
[13]	Liquid water surface tension (at 20 °C)	σ_w	N/m	72.7×10^{-3}
[13]	Liquid water viscosity (at 20 °C)	η_w	kg/(m s)	0.959×10^{-3}
[30]	Calcium silicate density (dry)	ρ_{dry}	kg/m^3	333
[34]	Calcium silicate heat capacity (dry)	$c_{p,dry}$	J/(kg °C)	1000
[30]	Calcium silicate free sat. water content	u_f	kg/m^3	850
[30]	Thermal conductivity rad. parameter	C	W/(m K^4)	1.11×10^{-11}
[30]	Thermal conductivity of the solid matrix	λ_{sm}	W/(m K)	0.2974
[30]	Thermal conductivity parameter	a	–	0.18839
[29]	Diffusion resistance (dry)	μ_{dry}	–	8.7
[29]	Diffusion resistance parameter	m	–	3.6287
[29]	Diffusion resistance parameter	n	–	1.9256
[29]	Moisture desorption parameter	k_1	Pa	6.44×10^5
[29]	Moisture desorption parameter	k_2	–	0.7649
[29]	Moisture absorption parameter	k_1	Pa	8.48×10^3
[29]	Moisture absorption parameter	k_2	–	0.5289
[30]	Water diffusivity parameter	ξ_1	m	5.1×10^{-11}
[30]	Water diffusivity parameter	ξ_2	m	2×10^{-8}
[30]	Water diffusivity parameter	ζ_1	–	−0.8
[30]	Water diffusivity parameter	ζ_2	–	8.1
[31]	Lewis number	Le	–	0.87

$$\lambda_{\text{eff}} = \frac{1}{\frac{1-a}{\lambda_I} + \frac{a}{\lambda_{\text{II}}}} \tag{B.4}$$

In order to complete the model, the following relations are needed:

$$\lambda_I = (1-\psi)\lambda_{\text{sm}} + \psi_w \lambda_w + (\psi - \psi_w)(\lambda_a + CT^3) \tag{B.5}$$

$$\lambda_{\text{II}} = \frac{1}{\frac{1-\psi}{\lambda_{\text{sm}}} + \frac{\psi_w}{\lambda_w} + \frac{(\psi-\psi_w)}{(\lambda_a + CT^3)}} \tag{B.6}$$

Eqs. (B.5) and (B.6) are appropriate when the fraction of closed cavities (i.e. not accessible to the moisture) is negligible if compared to the total pore volume. In case this condition does not apply, an extended model proposed by [47] can be used. The thermal conductivity of liquid water is calculated according to the following equation [48]:

$$\lambda_w = -0.90032 + 0.00839\ T - 1.11802 \times 10^{-5}\ T^2 \tag{B.7}$$

Finally, the surface tension σ_w and viscosity η_w of liquid water, appearing in Eq. (B.2), depend on the temperature according to e.g. [13]. The material properties and model parameters used for simulation are reported in Table B.1.

References

[1] W. Feist, Passivhauskomponenten und Innendämmung, Protokollband Nr. 32. Faktor 4 auch bei sensiblen Altbauten: Passivhauskomponeneten + Innendämmung, 2005, pp. 1–16.
[2] E. Vereecken, S. Roels, A comparison of the hygric performance of interior insulation systems: a hot box-cold box experiment, Energy Build. 80 (2014) 37–44.
[3] E. Vereecken, L. Van Gelder, H. Janssen, S. Roels, Interior insulation for wall retrofitting – a probabilistic analysis of energy savings and hygrothermal risks, Energy Build. 89 (2015) 231–244.
[4] H. Künzel, Simultaneous Heat and Moisture Transport in Building Components, Fraunhofer IRB Verlag Stuttgart, 1995 ISBN 3-8167-4103-7.
[5] P. Häupl, J. Grunewald, H. Fechner, H. Stopp, Coupled heat air and mois- ture transfer in building structures, Int. J. Heat Mass Transfer. 40 (7) (1997) 1633–1642.
[6] J. Grunewald, Diffusiver und konvektiver Stoff- und Energietransport in kapillarporösen Baustoffen (PhD thesis), Technischen Universität Dresden, 1997.
[7] P. Baggio, C. Bonacina, B.A. Shrefler, Some considerations on modeling heat and mass transfer in porous media, Transp. Porous Media 28 (1997) 233–251.
[8] P. Häupl, H. Fechner, Hygric material properties of porous building materials,
J. Build. Phys. 26 (3) (2003) 259–284.
[9] G.A. Scheffler, Validation of Hygrothermal Material Modelling Under Consider- ation of the Hysteresis of Moisture Storage (PhD thesis), Technischen Univer- sität Dresden, 2008.
[10] S. Roels, J. Carmelit, H. Hens, O. Adan, H. Brocken, R. Cerny, Z. Pavlik, C. Hall,
K. Kumaran, L. Pel, R. Plagge, Interlaboratory comparison of hygric properties of porous building materials, 2004 J. Therm. Envel. Build. Sci., 27 307–325.
[11] M. Van Belleghem, M. Steeman, H. Janssen, A. Janssens, M. De Paepe, Valida- tion of a coupled heat, vapour and liquid moisture transport model for porous materials implemented in CFD, Build. Environ. 81 (2014) 340–353.
[12] J. Zhao, R. Plagge, Characterization of hygrothermal properties of sandstones –impact of anisotropy on their thermal and moisture behaviors, Energy Build. 107 (2015) 479–494.
[13] O. Krischer, Die wissenschaftlichen Grundlagen der Trocknungstechnik, second ed., Springer-Verlag, Berlin, 1963.
[14] L. Pel, H. Brocken, Determination of moisture diffusivity in porous media us- ing moisture concentration profiles, Int. J. Heat Mass Transfer 39 (6) (1996) 1273–1280.
[15] M. Krus, Moisture Transport and Storage Coefficients of Porous Mineral Building Materials – Theoretical Principles and New Test Methods, Fraunhofer IRB Verlag Stuttgart, 1996 ISBN 3-8167-4535-0.
[16] J. Carmeliet, H. Hens, S. Roels, O. Adan, H. Brocken, R. Cerny, Z. Pavlik, C. Hall,
K. Kumaran, L. Pel, Determination of the liquid water diffusivity from transient moisture transfer experiments, J. Build. Phys. 27 (4) (2004) 277–305.
[17] A. Tavukçuoglu, E. Grinzato, Determination of critical moisture content in porous materials by IR thermography, Quant. InfraRed Thermogr. J. 3 (2) (2006) 231–245.
[18] M. Bianchi Janetti, L.P. Colombo, F. Ochs, W. Feist, Determination of the wa- ter retention curve from drying experiments using infrared thermography: a preliminary study, Int. J. Therm. Sci. 114 (2017) 271–280.
[19] W. Masmoudi, M. Prat, Heat and mass transfer between a porous medium and a parallel external flow. Application to drying of capillary porous materials, Int.
J. Heat Mass Transfer 34 (8) (1991) 1975–1989.
[20] V.P. Chandra Mohan, P. Talukdar, Three dimensional numerical modeling of si- multaneous heat and moisture transfer in a moist object subjected to convec- tive drying, Int. J. Heat Mass Transfer 53 (21–22) (2010) 4638–4650.
[21] T. Defraeye, B. Blocken, J. Carmeliet, Analysis of convective heat and mass transfer coefficients for convective drying of a porous flat plate by conjugate modelling, Int. J. Heat Mass Transfer 55 (September) (2011) 112–124.
[22] C. James, C.J. Simonson, P. Talukdar, S. Roels, Numerical and experimental data set for benchmarking hygroscopic buffering models, Int. J. Heat Mass Transfer 53 (September) (2010) 3638–3654.

[23] M. Van Belleghem, M. Steeman, A. Willockx, A. Janssens, M. De Paepe, Bench- mark experiments for moisture transfer modelling in air and porous materials, Build. Environ. 46 (April) (2011) 884–898.
[24] T. Defraeye, B. Blocken, J. Carmeliet, Influence of uncertainty in heat-moisture transport properties on convective drying of porous materials by numerical modelling, Chem. Eng. Res. Des. 91 (1) (2013) 36–42.
[25] M. Van Belleghem, M. Steeman, A. Janssens, M. De Paepe, Drying behaviour of calcium silicate, Constr. Build. Mater. 65 (2014) 507–517.
[26] H. Janssen, G.A. Scheffler, R. Plagge, Experimental study of dynamic effects in moisture transfer in building materials, Int. J. Heat Mass Transfer 98 (2016) 141–149.
[27] P. Furmański, T. Wiśniewski, E. Wyszyńska, Detection of moisture in porous materials through infrared methods, Arch. Thermodyn. 29 (1) (2008) 19–40.
[28] E. Barreira, R.M.S.F. Almeida, J.M.P.Q. Delgado, Infrared thermography for as- sessing moisture related phenomena in building components, Constr. Build. Mater. 110 (2016) 251–269.
[29] M. Bianchi Janetti, Hygrothermal Analysis of Building Components Inclosing Air Cavities: Comparison between Different Modeling Approaches and Experi- mental Results (PhD thesis), Universität Innsbruck, 2015.
[30] M. Bianchi Janetti, T.A. Carrubba, F. Ochs, W. Feist, Heat flux measurements for determination of the liquid water diffusivity in capillary active materials, Int.
J. Heat Mass Transfer 97 (2016) 954–963.
[31] H.D. Baehr, K. Stephan, Wärme- und Stoffübertragung, Springer-Verlag, Berlin, 2008 6. ed..
[32] A.V. Luikov, Heat and Mass Transfer in Capillary-Porous Bodies, Pergamon Press, Oxford, 1966.
[33] O.A. Alduchov, R.E. Eskridge, Improved Magnus form approximation of satura- tion vapor pressure, J. Appl. Meteor. 35 (1995) 601–609.
[34] H. Fechner, U. Ruisinger, A. Nicolai, J. Grunewald, Delphin. Simulation Program for the Calculation of Coupled Heat, Moisture, Air, Pollutant, and Salt Transport, 2015 http://www.bauklimatik-dresden.de/delphin/index.php.
[35] H. Künzel, K. Kiessl, Calculation of heat and moisture transfer in exposed building components, Int. J. Heat Mass Transfer 40 (October) (1996) 159–167.
[36] A.W.M. Van Schijndel, Modeling and solving building physics problems with FemLab, Build. Environ. 38 (2) (2003) 319–327.
[37] A.W.M. Van Schijndel, Integrated modeling of dynamic heat, air and moisture processes in buildings and systems using SimuLink and COMSOL, Build. Simul. 2 (2009) 143–155.
[38] J.I. Knarud, S. Geving, Implementation and benchmarking of a 3D hygrothermal model in the COMSOL multiphysics software, Energy Proc. 78 (1876) (2015) 3440–3445.
[39] D. Lelievre, T. Colinart, P. Glouannec, Hygrothermal behavior of bio-based building materials including hysteresis effects: experimental and numerical analyses, Energy Build. 84 (2014) 617–627.
[40] C. Belleudy, M. Woloszyn, M. Chhay, M. Cosnier, A 2D model for coupled heat, air, and moisture transfer through porous media in contact with air channels, Int. J. Heat Mass Transfer 95 (2016) 453–465.
[41] M. Bianchi Janetti, F. Ochs, L.P.M. Colombo, Hygrothermal Modeling: A Numer- ical and Experimental Study on Drying, Comsol Conference München, 2016.
[42] M. Celia, E. Bouloutas, R. Zarba, A general mass-conservative numerical so- lution for the unsaturated flow equation, Water Resour. Res. 26 (7) (1990) 1483–1496.
[43] H. Janssen, B. Blocken, J. Carmeliet, Conservative modelling of the moisture and heat transfer in building components under atmospheric excitation, Int. J. Heat Mass Transfer 50 (March) (2007) 1128–1140.
[44] H. Janssen, Simulation efficiency and accuracy of different moisture transfer potentials, J. Build. Perform. Simul. 7 (5) (2013) 379–389.
[45] A. Holm, M. Krus, H. Künzel, Approximation der Feuchtespeicherfunktion aus einfach bestimmbaren Kennwerten, IBP-Mitteilung 406 29 (2002) 10–11.
[46] M. Van Belleghem, H.-J. Steeman, M. Steeman, A. Janssens, M. De Paepe, Sen- sitivity analysis of CFD coupled non-isothermal heat and moisture modelling, Build. Environ. 45 (11) (2010) 2485–2496.
[47] F. Ochs, W. Heidemann, H. Mullersteinhagen, Effective thermal conductivity of moistened insulation materials as a function of temperature, Int. J. Heat Mass Transfer 51 (2008 Feb) 539–552.
[48] M.L.V. Ramires, C.A. Nieto de Castro, Y. Nagasaka, A. Nagashima, M.J. Assael, W.A. Wakeham, Standard reference data for the thermal conductivity of water,
J. Phys. Chem. Ref. Data 24 (1995) 1377.